Universal relations to measure neutron star properties from targeted r-mode searches

Suprovo Ghosh 60 *

Inter-University Centre for Astronomy and Astrophysics, Pune University Campus, Pune 411007, India

Accepted 2023 July 31. Received 2023 July 31; in original form 2023 April 24

ABSTRACT

R-mode oscillations of rotating neutron stars (NS) are promising candidates for continuous gravitational wave (GW) observations. In our recent work, we derived universal relations between the NS parameters compactness and dimensionless tidal deformability with the r-mode frequency. In this work, we investigate how these universal relations can be used to infer various NS intrinsic parameters following a successful detection of the r-modes. In particular, we show that for targeted r-mode searches, these universal relations along with the 'I-Love-Q' relation can be used to estimate both the moment of inertia and the distance of the NS, thus breaking the degeneracy of distance measurement for continuous gravitational wave (CGW) observations. We also discuss that, with a prior knowledge of the distance of the NS from electromagnetic observations, these universal relations can also be used to constrain the dense matter equation of state (EOS) inside the NS. We quantify the accuracy to which such measurements can be done using the Fisher information matrix for a broad range of possible, unknown parameters for both the a-LIGO and Einstein Telescope (ET) sensitivities.

Key words: equation of state – gravitational waves – stars: oscillations – pulsars: general.

1 INTRODUCTION

The first detection of gravitational waves (GWs) from a binary black hole (BBH) merger event GW150914 (Abbott et al. 2016a) has opened up a new rapidly growing field in modern astrophysics. Since the first detection of a BBH merger in 2015, till now we have made almost 100 confirmed detections (Abbott et al. 2021a) of GWs from binary systems including binary neutron star (BNS; Abbott et al. 2017b) and neutron star-black hole (BH-NS; Abbott et al. 2021b) systems using the LIGO-Virgo-Kagra (LVK) global network of GW detectors (Acernese et al. 2014; Aasi et al. 2015; Abbott et al. 2016b; Akutsu et al. 2021). The BNS merger event GW170817 (Abbott et al. 2017b, 2018b, 2019) was also observed throughout the electromagnetic spectrum opening the modern era of multimessenger astronomy (Abbott et al. 2017c).

Although till now, we have only observed GW emission from binary sources, with increasing sensitivity of the current detectors and also the upcoming third-generation detectors like the Einstein telescope (Punturo et al. 2010; Hild et al. 2011) or the Cosmic Explorer (Abbott et al. 2017a), we will also possibly detect weaker sources of GWs, such as continuous gravitational waves (CGW) emission from spinning isolated neutron stars (NSs) is characterized by its long-lasting and almost monochromatic nature. Deformations or 'mountains' on the surface of NS supported by elastic and/or magnetic strain, rigid rotation of a triaxial star or fluid oscillations in a rotating NS are the main sources of CGW emission from NS (See Riles (2023) for a recent review).

* E-mail: suprovo@iucaa.in

R-mode is a toroidal mode of fluid oscillation for which the restoring force is the Coriolis force (Papaloizou & Pringle 1978; Andersson 1998; Friedman & Morsink 1998; Andersson 2003). For any rotating star, Chandrasekhar-Friedman-Schutz (Chandrasekhar 1970; Friedman & Schutz 1978) mechanism drives the r-mode unstable leading to GW emission. This instability can explain the spin-down of hot and young NSs (Lindblom, Owen & Morsink 1998; Andersson, Kokkotas & Schutz 1999a; Alford & Schwenzer 2014), as well as old, accreting NSs in low-mass X-ray binaries (Bildsten 1998; Andersson, Kokkotas & Stergioulas 1999b; Ho, Andersson & Haskell 2011). Because of the astrophysical significance, CGW emission from r-modes has been searched in the LVK data for the Crab pulsar (Rajbhandari et al. 2021) and PSR J0537-6910 Fesik & Papa (2020a, b); Abbott et al. (2021c). No CGWs were still detected in these searches, but upper limits on strain amplitude were obtained.

GW emission from binary systems allows to calculate the luminosity distance of the system from the measured GW parameters alone (Schutz 1986); that's why these systems are called 'standard siren'. Recently, Sieniawska & Jones (2021) showed that CGW emission from NS can't be used as standard sirens since the distance estimation is always degenerate by one of the unknown physical parameters: moment of inertia (MoI) or the r-mode amplitude, denoted by α (ellipticity, ϵ in the case of 'mountains'). In the specific case of r-modes from barotropic, slowly rotating NS, the frequency of the emitted GW actually depends on the structure of the NS (Lindblom, Mendell & Owen 1999; Lockitch, Andersson & Friedman 2000; Lockitch, Friedman & Andersson 2003). In our recent paper (Ghosh, Pathak & Chatterjee 2023), we improved the universal relation of the r-mode frequency with the NS compactness considering the Newtonian limits of the r-mode frequency and recent

multimessenger constraints on the NS EOS (Dietrich et al. 2020; Traversi, Char & Pagliara 2020; Pang et al. 2021; Ghosh et al. 2022a; Ghosh, Chatterjee & Schaffner-Bielich 2022b) and also derived the universal relation between r-mode frequency and dimensionless tidal deformability of the NS. The current most sensitive searches for rmode using the LVK detectors are targeted searches for which we know the rotation frequency of the pulsars and the search is within a band of a few Hz (Caride et al. 2019). In this paper, we show that for such targeted r-mode searches, from the measured frequency, we can determine the MoI of the system for a given EOS and then calculate the distance, thus breaking the degeneracy between MoI and distance. We further analyse the accuracy to which such measurements can be made with a-LIGO detector (Abbott et al. 2018a, 2020a) and third-generation detectors like the Einstein Telescope. In particular, we show how the uncertainty in the inclination angle (ι) will affect the distance measurement of the pulsar. Although we do not include simulations for the third-generation detector, Cosmic Explorer (Abbott et al. 2017a; Evans et al. 2021), but the results are expected to be qualitatively similar to the Einstein Telescope. We also discuss that if we assume the knowledge of the distance from prior EM observations, we can use the universal relations to measure the mass and MoI of the NS that can be used to constrain the EOS.

The structure of the article is as follows: in Section 2, we describe the formalism of CGW from r-modes and the universal relations for the r-mode frequency. We also estimate errors of relevant signal parameters using the Fisher matrix. The details of the measured NS parameters and corresponding errors are discussed in Section 3. In Section 4, we discuss the main assumptions considered in this study and their validity with current observation scenarios. In Section 5, we discuss the main implications and future aspects of this work.

2 METHOD AND FORMALISM

2.1 Continuous gravitational waves from r-modes

The strain amplitude for r-mode oscillations is parametrized by the dimensionless quantity α (Owen et al. 1998) and the corresponding CGW strain is given by (Owen 2010)

$$h_0 = \sqrt{\frac{512\pi^7}{5}} \frac{G}{c^5} (\alpha M R^3 \tilde{J}) \frac{1}{d} f_{\rm GW}^3, \tag{1}$$

where M, R are the mass and radius of the star, respectively, $f_{\rm GW}$ is the frequency of the GW, α is the r-mode saturation amplitude, and \tilde{J} is a dimensionless parameter that depends on the EOS of the NS (Owen et al. 1998),

$$\tilde{J} = \frac{1}{MR^4} \int_0^R \rho r^6 \, \mathrm{d}r,\tag{2}$$

where ρ is the density inside the NS.

Assuming the star is losing all of its rotational energy via r-mode emission and the constant r-mode saturation amplitude α , the frequency derivative can be written as (Riles 2023)

$$\dot{f}_{\rm GW} = -\frac{4096\pi^7}{25} \frac{G}{c^7} \frac{M^2 R^6 \tilde{J}^2}{I} \alpha^2 f_{\rm GW}^7,\tag{3}$$

where I is the MoI of the NS. Eliminating the highly uncertain parameter $\alpha MR^3\tilde{J}$ from equations (1) and (3), we have

$$\frac{\sqrt{I}}{d} = h_0 \sqrt{\frac{f_{\rm GW}}{\dot{f}_{\rm GW}}} \sqrt{\frac{8c^3}{45G}}.$$
 (4)

This means that, unlike the binary inspirals (Schutz 1986), we cannot directly solve for distance (*d*) from the GW measurement alone, and it will always be degenerate with the MoI (*I*) (Sieniawska & Jones 2021).

2.2 Universal relations

For slowly and uniformly rotating barotropic stars, the r-mode frequency is proportional to the rotational frequency of the NS (Idrisy, Owen & Jones 2015; Ghosh et al. 2023),

$$f_{\rm GW} = |2 - \kappa| f_{\rm rot},\tag{5}$$

where $f_{\rm rot}$ is the rotational frequency of the star and κ is a dimensionless parameter. Idrisy et al. (2015) showed that κ has a universal relation with the NS compactness (C), which we improved considering a chosen set of 15 tabulated EOSs that are consistent with the recent multimessenger observations of NS and the Newtonian limits of the r-mode frequency (Ghosh et al. 2023)

$$\kappa = 0.667 - 0.478C - 1.11C^2. \tag{6}$$

We also showed that κ has a universal relation with the dimensionless tidal deformability (Λ) (Ghosh et al. 2023)

$$\kappa = 0.3612 + 0.0407 \log(\Lambda) - 0.0015 \log^2(\Lambda). \tag{7}$$

For slowly rotating stars, there are also universal relations between the NS MoI, the Love numbers, and the quadrupole moment called the I-Love-Q relations (Yagi & Yunes 2013b). The universal relation between the normalized MoI ($\bar{I} = I/m^3$) and tidal deformability is given by (Yagi & Yunes 2013a)

$$\ln(\bar{I}) = 1.47 + 0.0817 \ln(\Lambda) + 0.0179 \ln(\Lambda)^{2} + 2.87$$
$$\times 10^{-4} \ln(\Lambda)^{3} - 3.64 \times 10^{-5} \ln(\Lambda)^{4}. \tag{8}$$

2.3 Signal model and error estimation using Fisher matrix

The strain produced in a detector by the CGW signal from the r-mode oscillations in NS can be represented in the form of (Jaranowski, Królak & Schutz 1998)

$$h(t) = \sum_{i=1}^{4} \mathcal{A}^{i} h_{i}(t; \lambda)$$
(9)

in terms of four signal-amplitudes \mathcal{A} independent of the detector and the detector-dependent basis $h(t;\lambda)$. The signal amplitudes \mathcal{A}^i can be expressed in terms of the two polarization amplitudes A_+ , A_\times , the initial phase Ψ_0 and the polarization angle ψ . The additional parameters, represented by λ in equation (9), which modify the phase of the signal, include the star's sky location, detector position and, if the star is in a binary system, its orbital parameters. The polarization amplitudes A_+ and A_\times can be written in terms of the characteristic amplitudes h_0 and the inclination angle ι between the NS's rotation axis to the line of sight (Jaranowski et al. 1998)

$$A_{+} = \frac{1}{2}h_{0}(1 + \cos^{2}\iota) \quad A_{\times} = h_{0}\cos\iota. \tag{10}$$

To express the phase of the CGW signal, we assumed that in the rest frame of the NS, the GW frequency can be expanded in a Taylor series. For the case of targeted searches (which is also what we are considering in this work for the most sensitive r-mode searches), the sky location of the source is known, and the phase can be expressed as a polynomial function of the initial phase (Ψ_0) , frequency, and the

higher order derivatives (Jaranowski & Królak 1999),

$$\Psi = \Psi_0 + 2\pi \left[ft + \frac{1}{2} \dot{f} t^2 + \frac{1}{6} \ddot{f} t^3 \right],\tag{11}$$

where t is an arbitrary time and Ψ_0 is the initial phase, which is set to be zero. The parameter space metric over the phase parameter set $\mathcal{P} = (f, \dot{f}, \ddot{f})$ can be written as

$$g_{ij} = \left\langle \frac{\partial \Psi}{\partial f^{(i)}} \frac{\partial \Psi}{\partial f^{(j)}} \right\rangle - \left\langle \frac{\partial \Psi}{\partial f^{(i)}} \right\rangle \left\langle \frac{\partial \Psi}{\partial f^{(j)}} \right\rangle, \tag{12}$$

where $(f^{(0)}, f^{(1)}, f^{(2)}) = (f, \dot{f}, \dot{f})$. The Fisher Co-variance matrix is given by the inverse of the above matrix

$$\Gamma = \frac{g^{-1}}{\rho^2},\tag{13}$$

where ρ^2 is the signal-to-noise ratio (SNR) assuming optimal match between the true signal and the best-fit template (Moore, Cole & Berry 2014). The SNR is calculated using the formula

$$\rho^2 = \int_0^\infty \frac{4|\tilde{h}(f)|^2}{S_n(f)} \, \mathrm{d}f,\tag{14}$$

where $\tilde{h}(f)$ is a Fourier transform of the GW signal and $S_n(f)$ is the amplitude spectral density, which determines the sensitivity of the detector. For observation times of one year or more, we can get an expression for SNR averaged over the sky location and polarization angle ψ (Jaranowski et al. 1998)

$$\rho^2 = \frac{1}{40} \frac{h_0^2 T}{S_n(f)} (1 + 6\cos^2 \iota + \cos^4 \iota), \tag{15}$$

and if we further average over inclination angle $\cos \iota \in [-1, 1]$, then we get (Prix 2007),

$$\rho^2 = \frac{4}{25} \frac{h_0^2 T}{S_n(f)}. (16)$$

The error propagation for any physical quantity that depends on our parameter set $\mathcal{P} = (h_0, f, \dot{f}, \dot{f})$ can be written as

$$\sigma(A)^{2} = \sum_{x,y \in \mathcal{D}} \left(\frac{\partial A}{\partial x}\right) \left(\frac{\partial A}{\partial y}\right) \Gamma_{xy},\tag{17}$$

where Γ_{xy} denotes the co-variance between the variables x, y. The error for the frequency and spin-down parameters can be obtained by evaluating equation (12) with the expression for the phase Ψ given in equation (11). For the amplitude parameters, only h_0 parameter is of importance to infer the NS interior properties. For targeted and year-long searches, we can consider the error in h_0 averaged over sky position and polarization angle ψ but dependent of the inclination angle ι ,

$$\frac{\sigma(h_0)}{h_0} = \frac{2a}{5\rho} \frac{\sqrt{b + \cos^2 i}}{1 - \cos^2 i},\tag{18}$$

where $a \approx 4.08$ and $b \approx 2.59$ (Prix 2007; Lu et al. 2023). Due to the singularity in the coordinate transformation between the four amplitude parameters A_i and $\{h_0, \iota, \psi, \Psi_0\}$, there is a divergence in the error in equation (18) for $\cos \iota = \pm 1$ (Prix 2007). Using the formula (17), we get the error estimates for the quantity $\frac{d}{\sqrt{I}}$ from the equation (4) (Sieniawska & Jones 2021).

$$\sigma \left(\frac{d}{\sqrt{I}}\right)^{2} = \frac{45G}{8c^{3}} \frac{1}{(\pi \rho h_{0})^{2}} \left[\frac{75}{T} \frac{\dot{f}}{f^{3}} + \frac{1620}{T^{4} f \dot{f}} + \frac{675}{T^{3} f^{2}} + \pi^{2} \frac{\dot{f}}{f} \frac{2a}{5} \frac{\sqrt{b + \cos^{2} i}}{1 - \cos^{2} i}\right].$$
(19)

The parameter κ is calculated from the measured GW frequency $(f_{\rm GW})$ using the equation (5). The error in measuring the parameter κ is estimated by

$$\sigma(\kappa)^2 = \left(\frac{f_{\rm GW}}{f_{\rm rot}}\right)^2 \left[\left(\frac{\sigma(f_{\rm GW})}{f_{\rm GW}}\right)^2 + \left(\frac{\sigma(f_{\rm rot})}{f_{\rm rot}}\right)^2 \right]. \tag{20}$$

From the universal relations in equations (7) and (8), we can estimate the error in the normalized MoI to be

$$\frac{\sigma(\bar{I})^2}{\bar{I}^2} = \left[(0.0817 + 0.0358ln\Lambda + 0.0008ln\Lambda^2 - 0.0002ln\Lambda^3) \right] \times \sigma(\kappa)^2 \frac{1}{0.0049 - 0.008\kappa}, \tag{21}$$

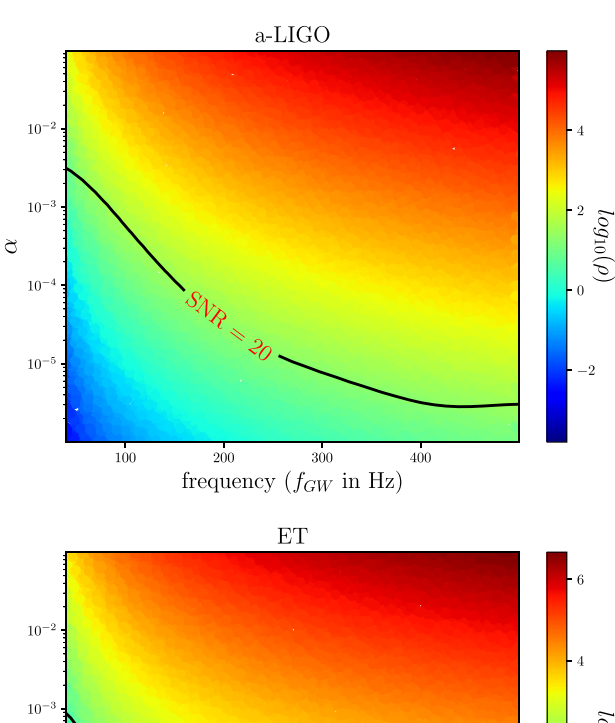
which can be converted into $\sigma(I)/I$ for a given EOS. Now, the error is measuring the distance can be simply calculated from equations (21) and (19)

$$\left(\frac{\sigma(d)}{d}\right)^2 = \left(\frac{\sigma(d/\sqrt{I})}{d/\sqrt{I}}\right)^2 + \frac{1}{4}\left(\frac{\sigma(I)}{I}\right)^2. \tag{22}$$

3 RESULTS

We first consider the SNR for simulated signals to calculate the detectability and the corresponding errors of the NS parameters associated with possible r-mode detection using the current and future generation GW detectors. To generate the signal model, we consider a canonical NS (Owen et al. 1998) with mass M = 1.4 M_{\odot} , $R = 12.53 \,\mathrm{km}$, $\tilde{J} = 0.0163$, and $I = 10^{38} \,\mathrm{kg} \,\mathrm{m}^2$ at a distance d = 1 kpc. We consider the r-mode saturation amplitude α in the theoretical expected range of 10^{-6} – 10^{-1} (Arras et al. 2003: Bondarescu, Teukolsky & Wasserman 2009) and the CGW frequency in the range of 40-500 Hz. We don't go up to very high frequency because the universal relations used in our study are not valid for very fast rotating NS (Doneva et al. 2013; Idrisy et al. 2015). We simulate the CGW signals for this wide range of parameters for the NS with an observing period of 2 years, which matches the duration of the future LVK observing runs, and calculate the expected SNR denoted by ρ , using the formula given in equation (16) averaged over sky location, polarization angle, and inclination angle. In Fig. 1, we plot the SNR for both a-LIGO and ET design sensitivity curves and see that for third generation detector ET, the SNR is an order of magnitude higher, as expected. Considering a minimum SNR of 20 is required for a signal to be detectable, we see that a canonical NS at a distance 1 kpc with r-mode frequency \geq 100 Hz and $\alpha \geq$ 10⁻⁴ will be detectable with 2 years of observing using the third generation GW detector ET. The SNR estimates shown in this figure also re-scale accordingly with changing distances.

If we want to measure distance of the NS from the detected signal, we need to first estimate the MoI to break their degeneracy, as shown in equation (4). In the case of targeted searches for detectable signals, we will be able to determine the value of r-mode frequency ($f_{\rm GW}$) with a great accuracy from the phase of the signal (Jaranowski & Królak 1999) and subsequently the value of κ using the equation (5). Assuming the sources are slowly rotating NS, we can use the universal relations given in equations (7) and (8) to estimate the tidal deformability (Λ) and normalized MoI (\bar{I}), respectively. To estimate the MoI from the normalized MoI (\bar{I}), we need to assume a true EOS of the NS matter, which allows us to calculate the mass of the star from the estimated tidal deformability. For this analysis, we choose four tabulated EOSs: WFF1, APR4, SLY9, and GM1, among which WFF1 and GM1 are the softest and stiffest EOS, respectively. All our EOS tables are obtained from either CompOSE



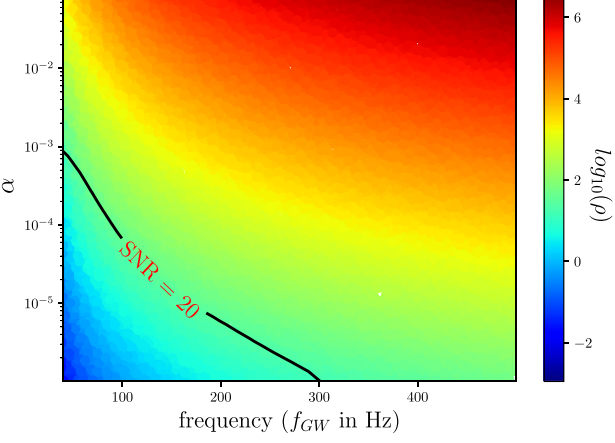


Figure 1. Expected SNR (ρ) for a wide range of possible α and f_{GW} values at a fixed distance = 1 kpc for two different GW detectors: a-LIGO (on the top) and ET (on the bottom). Solid black lines denote contour levels at SNR = 20.

(Oertel et al. 2017) or an EOS catalogue from Özel & Freire (2016) used in LALSuite (LIGO Scientific Collaboration 2018). All the EOSs satisfy the constraints of maximum mass $\geq 2\,\mathrm{M}_\odot$, 90 per cent tidal deformability limits from GW170817 (except the very stiff EOS GM1) and the M–R estimates from the NICER measurements (Abbott et al. 2020b; Biswas 2022). For these four chosen EOSs, we calculate the MoI using the universal relations and plot them as a function of κ in Fig. 2. For stiff EOSs GM1 and SLY9, we see the unstable branch (starting point is denoted by black dots in Fig. 2) determined by 'turning point' method (Friedman, Ipser & Sorkin 1988) at low values of κ , which corresponds to a high value of compactness that cannot be obtained for stable NSs with these stiff EOSs.

For the error measurement of the MoI, we assume a fixed pulsar at a distance d=1 kpc with $\alpha=10^{-3}$ and consider signals with SNR >20 for the ET design sensitivity so that the signals are detectable. As given in equation (21), for the error in measurement of I, we also require the values of κ , error in measurement of f_{rot} , and the choice of EOS. For targeted searches, we generally can measure the rotational frequency (f_{rot}) of the pulsar from prior EM observations up to a very high precision (Manchester et al. 2013; Desvignes et al. 2016),

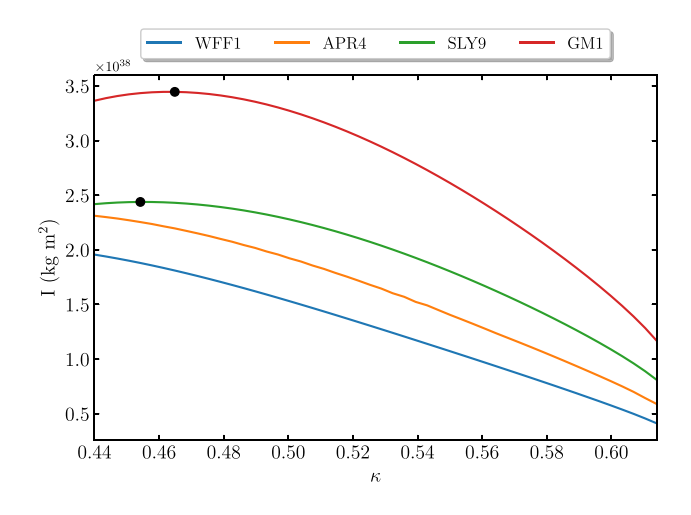


Figure 2. Estimated MoI as a function of κ for four different choice of EOS.

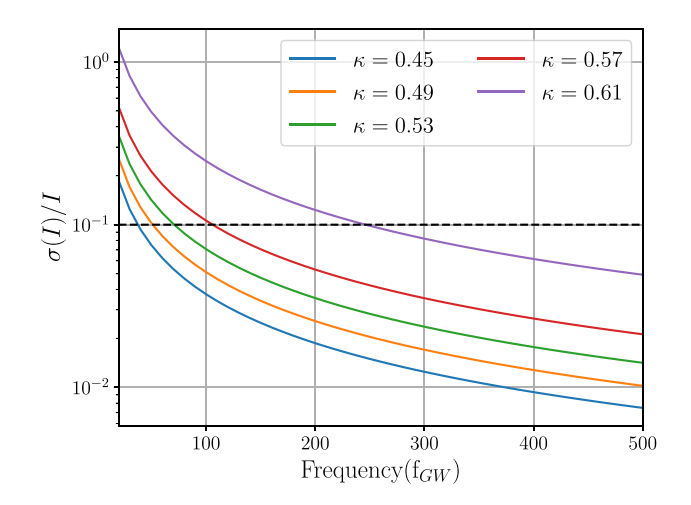


Figure 3. Error estimation of the MoI at a fixed value of distance d=1 kpc with $\alpha=10^{-3}$ for ET design sensitivity curve for SLY9 EoS. The dashed black lines denote a fixed value of relative error of 10 per cent.

although we consider here an error of 1 per cent. In Fig. 3, we plot the error in measuring the parameter I as a function of $f_{\rm GW}$ for different choices of κ for the particular EOS, SLY9. We see that the relative error decreases with a higher κ value but don't see much change in the error estimation with different EOSs (figures not shown). Also, we observe that for reasonable values of κ (Ghosh et al. 2023), we can measure the MoI up to 10 per cent accuracy for CGW frequency \geq 100 Hz. We also find that the relative errors will increase with increasing distance and decreasing α (Figures not shown), which is also evident from equation (1) and Fig. 1, respectively.

Although we can estimate the MoI from the frequency measurement using the universal relation, to get the distance of the pulsar, we need to estimate the characteristic amplitude h_0 . The differing amplitudes of the two polarizations of the gravitational waveforms A_+ and A_\times allow us to determine both the binary inclination (ι) and the characteristic amplitude h_0 from equation (10). However, both polarizations have nearly identical amplitudes at small inclination angles (difference less than 5 per cent for $\iota \leq 45^\circ$) and significantly lower amplitudes at large inclination angles (Usman, Mills & Fairhurst 2019). This leads to the conclusion that

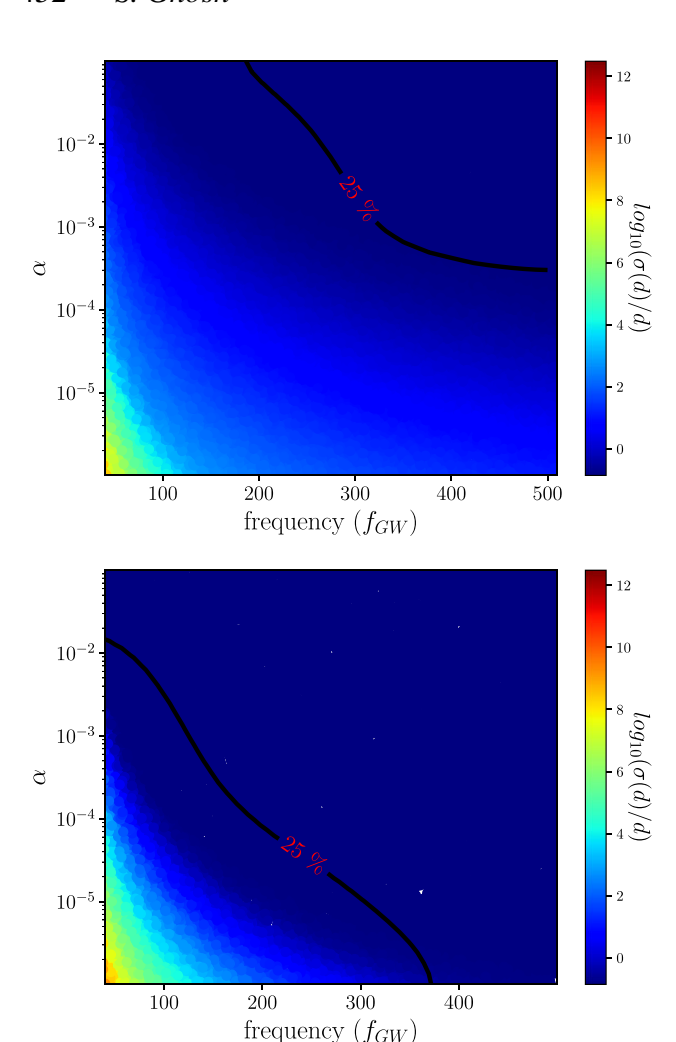


Figure 4. Error estimation of d for a wide range of possible α and $f_{\rm GW}$ values at fixed value of d=1 kpc for ET design sensitivity for two different inclination angle: $\iota \sim 0^\circ$ (on the top) and $\iota \sim 90^\circ$ (on the bottom). The solid black lines denote contours of relative error of 25 per cent.

the CGW signal is strongest for NSs that are close to face-on ($\iota\sim0^\circ)$ or face-away ($\iota\sim180^\circ)$, and thus there is an observational bias towards detecting NSs whose orbital angular momentum is well aligned (or anti-aligned) with the line of sight. In that case, if the amplitudes of the two polarizations are close to equal, we cannot measure strain amplitude or inclination separately. This will lead to a degeneracy between the distance estimation with the inclination angle of the NS, which is also present in the case of binary systems (Nissanke et al. 2010; Schutz 2011).

To look into the effect of uncertainty of the inclination angle on the distance measurement in Fig. 4, we plot the error in measurement of d as a function of α varied in the range of 10^{-6} – 10^{-1} and the CGW frequency to be in the range of 40– $500\,\mathrm{Hz}$ for two different inclinations: $\iota \sim 0^\circ$ and 90° . A canonical NS at a distance of 1 kpc with 'SLY9' EOS and fixed $\kappa = 0.5$ was considered for the ET design sensitivity. In Fig. 4, we also show the contour of 25 per cent relative error in measured distance in black solid lines. For a pulsar at d = 1 kpc aligned with the line of sight, for detectable signals, we can measure the distance up to an accuracy of 25 per cent for $f_{\mathrm{GW}} \geq 300\,\mathrm{Hz}$ and $\alpha \geq 10^{-3}$, but the errors decrease when the inclination angle changes to $\iota \sim 90^\circ$. Although SNR decreases with increasing

inclination angle changes from $\iota \sim 0^\circ$ to 90° (from equation (15)), since the measurement of h_0 becomes degenerate with inclination angle at low values, the error in measuring h_0 and hence, distance (d) become larger at low inclination angles. These error estimates also scale accordingly with changing distance of the pulsar (figures not shown).

4 ASSUMPTIONS

In this section, we revisit some of the assumptions we made for our analysis. Throughout our calculation, we have assumed the entire spin-down is driven by CGW emission via r-modes. This is, of course, not true for targeted searches since we already observe them as pulsars and so, only a fraction of the spin-down energy is radiated by CGW emission. A measurement of braking index, $n = \frac{f \, \tilde{f}}{\ell}$, can differentiate between the spin-down mechanisms; for example, n =3 indicates dipole emission and n = 7 for r-mode emission (Riles 2023). Recent analysis of PSR J0537 measures a braking index n \approx 7, which indicates that a significant fraction of the spin-down energy is radiated via r-modes (Andersson et al. 2018). That is also what makes this pulsar the most promising candidate for r-mode searches. It may in fact be possible to carry out an analysis assuming an electromagnetic component to the spin-down, as described in Lu et al. (2023). From a successful CGW detection, we will also be able to measure the braking index with great accuracy, which can shed light to the various spin-down components (Sieniawska & Jones 2021).

While considering the phase of the signal model in (11), we ignored the dependence of the signal on the source's sky location (Jaranowski & Królak 1999). For targeted searches, we have prior knowledge about the sky location of the source, and also in general in CGW observations, the sky location is expected to be measured extremely accurately. In practice, we should also consider the effect of cosmological parameters such as redshift (z) on the detectability of the signals, especially when trying to estimate distances. But Sieniawska & Jones (2021) showed that percentage change in the CGW amplitude estimation due to the cosmological corrections is within a few percents and so will not be very important for such detection. To estimate the errors, rather than a full Bayesian analysis, we use the Fisher information matrix formalism, which is strictly valid only in the case of high SNRs and also has several other limitations (Vallisneri 2008). Still, we adapt this formalism because it is computationally easy to implement and gives a qualitative accurate estimation of the inferred parameters.

While considering the signal strain amplitude, we considered a constant value of r-mode amplitude α . If the NS is spinning down via r-mode emission, r-mode amplitude will grow due to the CFS mechanism (Chandrasekhar 1970; Friedman & Schutz 1978) till it reaches a constant value called saturation amplitude α_s due to dynamical couplings with other modes (Arras et al. 2003). In our model, we assumed a constant value of α_s similar to Owen et al. (1998), but different studies indicate more complex behaviour with different limits to the value of α_s (Arras et al. 2003; Brink, Teukolsky & Wasserman 2004; Bondarescu et al. 2009). An upper limit of this saturation amplitude was also obtained from the non-detection of r-modes from PSR J0537 using recent analysis of the O3 data (Abbott et al. 2021c).

The universal relations used in this paper are also valid under some specific conditions. The universal relations obtained in our recent work Ghosh et al. (2023) are valid for slow rotation limits only. The higher order effect is of the order of $\left(\frac{f}{f_{\rm K}}\right)^2$ (Idrisy et al. 2015),

where $f_{\rm K}$ is the Keplerian frequency ($\propto \sqrt{M/R^3}$). The 'I–Love–Q' relations also do not hold true for rapidly rotating stars (Doneva et al. 2013) or highly magnetized stars (Haskell et al. 2013) and become EOS dependent. There are several other factors like the presence of a solid crust (Levin & Ushomirsky 2001), stratification (Yoshida & Lee 2000; Passamonti et al. 2009; Gittins & Andersson 2023), magnetic field (Ho & Lai 2000; Rezzolla, Lamb & Shapiro 2000; Rezzolla et al. 2001a, b; Morsink & Rezania 2002), or superfluidity in the core (Lindblom & Mendell 2000; Andersson & Comer 2001) that might affect the r-mode frequency, but their effect was found to be negligible for most stars (Idrisy et al. 2015). The most promising target PSR J0537-6910 has rotational frequency = 62 Hz (Marshall et al. 1998), which determines r-mode frequency in the range of 86-99 Hz (Ghosh et al. 2023), much lower than its Keplerian frequency. So, for a future detection of r-mode from this particular pulsar, we can use both the universal relations to infer the NS intrinsic properties.

5 DISCUSSION AND CONCLUSION

In this work, we showed how to measure the various NS intrinsic properties from a future successful r-mode detection using the current and third generation GW detectors. We mainly focused on how to break the degeneracy between the MoI and distance measurement from a r-mode detection that was recently pointed out in Sieniawska & Jones (2021). Using the universal relations obtained in our earlier work (Ghosh et al. 2023) for targeted pulsars, we can measure the compactness and the dimensionless tidal deformability from the measured CGW frequency. Using the 'I-love-Q' relations, we can then calculate the normalized MoI, and knowledge of the true EOS allows to calculate the MoI (I) of the system. Stiffer EOS predicts a higher value of MoI, which is expected as stiffer EOS predicts a higher radius for a NS. Once the MoI is known, we can easily calculate the distance (d) from the measured strain amplitude (h_0) . This way, from the measurement of the characteristic strain amplitude (h_0) and the CGW frequency (f_{GW}) , we can measure the distance of the pulsar using these continuous gravitational observations and break the degeneracy with MoI. But this way of distance measurement still suffers from its degeneracy with inclination angle similar to binary GW observations (Nissanke et al. 2010; Schutz 2011). In future, the network of five detectors with the recent addition of KAGRA (Aso et al. 2013) and the upcoming LIGO-India (Saleem et al. 2021) or the triangular configuration of the ET (Punturo et al. 2010) would further increase the network's sensitivity to constrain both the inclination angle and distance (Usman et al. 2019). Electromagnetic observations of the pulsars can also be used to constrain the inclination angle and thus breaking their degeneracy with distance (Benli, Pétri & Mitra 2021).

Although we can calculate the MoI up to 10 per cent accuracy for CGW signals from a pulsar at d=1 kpc with frequency ≥ 100 Hz; the distance estimation, being dependent on the measurement of h_0 has much larger errors and also suffers from its degeneracy with the inclination angle. For pulsars aligned with line of sight, to have below 25 per cent accuracy in the distance estimation with CGW frequency ≥ 300 Hz, we need $\alpha \geq 10^{-3}$. Recent limits on the r-mode saturation amplitudes (Bondarescu et al. 2009; Haskell, Glampedakis & Andersson 2014) suggest that we might need much longer observation periods than considered here with third generation GW detectors to achieve this accuracy. For nearby pulsars, we expect a detection from a shorter observing period with errors in distance measurement comparable to the same from EM observations of pulsars (Kaplan et al. 2008). Recently, Sieniawska, Jones & Miller (2023) discussed the measurement of distance from CGW

observations using the parallax method. Although this parallax method does not require any prior EM knowledge of the pulsar to calculate distance, with this method we can measure distances up to very nearby pulsars (up to a few hundreds of parsecs) with sufficient accuracy (Sieniawska et al. 2023). Although, unlike the case of binary systems, we need a prior knowledge of the star's rotational frequency from EM observations and the assumption of a true EOS, with the sensitivity of the current searches, this method gives an alternative way to calculate the pulsar distances from CGW observations alone.

Another alternate way to use the universal relations is to constrain the NS EOS with the prior knowledge of the distance for the targeted pulsars from EM observations. For the recent r-mode targeted pulsars, PSR J0537-6910 (Abbott et al. 2021c) or the Crab pulsar (Rajbhandari et al. 2021), we know their distance with good accuracy from the pulsar timing data (Kaplan et al. 2008; Pietrzyński et al. 2019). Measurement of the MoI of the NS using prior knowledge of distance and normalized MoI from the CGW frequency using the universal relations as described in Section 3 allows to measure the mass of the NS also (See fig. 19 for upper limits of the mass estimated from the recent O3 analysis of PSR J0537 by the LVK collaboration (Abbott et al. 2021b)). A separate MoI measurement from these r-mode CGW observations, along with mass measurements, can constrain the dense matter EOS inside NS (Bejger & Haensel 2003). It can also be used to check the validity of the 'I-Love-O' relation. which also carries the signatures of quark matter inside the NS (Yagi & Yunes 2013a, 2017). This kind of inference also relies on the assumption of saturated r-mode driven spin-down and an accurate measurement of the inclination angle from the CGW detection.

Future work could extend to a much more realistic model of r-mode oscillation inside the NS, considering both the growth and saturation of r-modes. According to Sieniawska & Jones (2021), a time-varying α could also be easily implemented in the energy conservation equations. Recent studies by Andersson & Gittins (2022) and Gittins & Andersson (2023) also emphasizes on the importance of composition stratification in a mature NS for the r-mode oscillations. Also, we should consider the parameter estimation in a full Bayesian framework to give robust conclusions about the inferred NS parameters as well as to use the prior information from the electromagnetic observations of NSs in a consistent way.

ACKNOWLEDGEMENTS

I would like to thank the anonymous referee for the useful comments and suggestions that have helped improve the paper. I would like to thank Prof. Debarati Chatterjee for her encouragement, useful comments and discussions during this work. I would like to thank Bikram Keshari Pradhan and Dhruv Pathak for various discussions during this work. I also acknowledge the usage of the IUCAA HPC computing facility, PEGASUS for the numerical calculations.

DATA AVAILABILITY

The data underlying this article will be shared on reasonable request to the corresponding author.

REFERENCES

Aasi J. et al., 2015, Class. Quantum Gravity, 32, 074001 Abbott R. et al., 2016a, Phys. Rev. Lett., 116, 061102 Abbott B. P. et al., 2016b, Phys. Rev. Lett., 116, 131103 Abbott B. P. et al., 2017a, Class. Quantum Gravity, 34, 044001

- 454 S. Ghosh Abbott B. et al., 2017b, Phys. Rev. Lett., 119, 161101 Abbott B. et al., 2017c, ApJL, 848, L12 Abbott B. P. et al., 2018a, Updated Advanced LIGO sensitivity design curve, Available from https://dcc.ligo.org/LIGO-T1800044/public [accessed 30 Mar 20181. Abbott B. et al., 2018b, Phys. Rev. Lett., 121, 161101 Abbott B. et al., 2019, Phys. Rev. X, 9, 011001 Abbott R. et al., 2020a, Living Rev. Relativ., 23, 3 Abbott B. et al., 2020b, Class Quantum Gravity, 37, 045006 Abbott R. et al., 2021a, Phys. Rev. X, 11, 021053 Abbott R. et al., 2021b, ApJL, 915, L5 Abbott R. et al., 2021c, ApJ, 922, 71 Acernese F. et al., 2014, Class. Quantum Gravity, 32, 024001 Akutsu T. et al., 2021, Prog. Theor. Exp. Phys., 2021, 05A101 Alford M. G., Schwenzer K., 2014, ApJ, 781, 26 Andersson N., 1998, ApJ, 502, 708
- Andersson N., 2003, Class. Quantum Gravity, 20, R105 Andersson N., Comer G., 2001, MNRAS, 328, 1129 Andersson N., Gittins F., 2022, ApJ, 945, 139
- Andersson N., Kokkotas K., Schutz B. F., 1999a, ApJ, 510, 846 Andersson N., Kokkotas K. D., Stergioulas N., 1999b, Astrophys. J., 516, 307
- Andersson N., Antonopoulou D., Espinoza C. M., Haskell B., Ho W. C. G., 2018, ApJ, 864, 137
- Arras P., Flanagan E. E., Morsink S. M., Schenk A. K., Teukolsky S. A., Wasserman I., 2003, ApJ, 591, 1129
- Aso Y., Michimura Y., Somiya K., Ando M., Miyakawa O., Sekiguchi T., Tatsumi D., Yamamoto H., 2013, Phys. Rev. D, 88, 043007
- Beiger M., Haensel P., 2003, Astron. Astrophys., 405, 747
- Benli O., Pétri J., Mitra D., 2021, A&A, 647, A101
- Bildsten L., 1998, Astrophys. J. Lett., 501, L89
- Biswas B., 2022, ApJ, 926, 75
- Bondarescu R., Teukolsky S. A., Wasserman I., 2009, Phys. Rev. D, 79,
- Brink J., Teukolsky S. A., Wasserman I., 2004, Phys. Rev. D, 70, 121501 Caride S., Inta R., Owen B. J., Rajbhandari B., 2019, Phys. Rev. D, 100, 064013
- Chandrasekhar S., 1970, Phys. Rev. Lett., 24, 611
- Desvignes G. et al., 2016, MNRAS, 458, 3341
- Dietrich T., Coughlin M. W., Pang P. T. H., Bulla M., Heinzel J., Issa L., Tews I., Antier S., 2020, Sci., 370, 1450
- Doneva D. D., Yazadjiev S. S., Stergioulas N., Kokkotas K. D., 2013, ApJL, 781, L6
- Evans M. et al., 2021, A Horizon Study for Cosmic Explorer: Science, Observatories, and Community, preprint (arXiv:2109.09882)
- Fesik L., Papa M. A., 2020a, ApJ, 895, 11
- Fesik L., Papa M. A., 2020b, ApJ, 897, 185
- Friedman J. L., Morsink S. M., 1998, Astrophys. J., 502, 714
- Friedman J. L., Schutz B. F., 1978, ApJ, 222, 281
- Friedman J. L., Ipser J. R., Sorkin R. D., 1988, ApJ, 325, 722
- Ghosh S., Pradhan B. K., Chatterjee D., Schaffner-Bielich J., 2022a, Front. Astron. Space Sci., 9, 864294
- Ghosh S., Chatterjee D., Schaffner-Bielich J., 2022b, Eur. Phys. J. A, 58, 37
- Ghosh S., Pathak D., Chatterjee D., 2023, ApJ, 944, 53
- Gittins F., Andersson N., 2023, MNRAS, 521, 3043
- Haskell B., Ciolfi R., Pannarale F., Rezzolla L., 2013, MNRAS: Lett., 438,
- Haskell B., Glampedakis K., Andersson N., 2014, MNRAS, 441, 1662
- Hild S. et al., 2011, Class. Quantum Gravity, 28, 094013
- Ho W. C. G., Lai D., 2000, ApJ, 543, 386
- Ho W. C. G., Andersson N., Haskell B., 2011, Phys. Rev. Lett., 107, 101101

- Idrisy A., Owen B. J., Jones D. I., 2015, Phys. Rev. D, 91, 024001 Jaranowski P., Królak A., 1999, Phys. Rev. D, 59, 063003 Jaranowski P., Królak A., Schutz B. F., 1998, Phys. Rev. D, 58, 063001 Kaplan D. L., Chatterjee S., Gaensler B. M., Anderson J., 2008, ApJ, 677,
- LIGO Scientific Collaboration, 2018, LIGO Algorithm Library—LALSuite, free software (GPL). Available at:https://lscsoft.docs.ligo.org/lalsuite/lal suite/index.html
- Levin Y., Ushomirsky G., 2001, MNRAS, 324, 917
- Lindblom L., Mendell G., 2000, Phys. Rev. D, 61, 104003
- Lindblom L., Owen B. J., Morsink S. M., 1998, Phys. Rev. Lett., 80, 4843
- Lindblom L., Mendell G., Owen B. J., 1999, Phys. Rev. D, 60, 064006
- Lockitch K. H., Andersson N., Friedman J. L., 2000, Phys. Rev. D, 63, 024019
- Lockitch K. H., Friedman J. L., Andersson N., 2003, Phys. Rev. D, 68, 124010
- Lu N., Wette K., Scott S. M., Melatos A., 2023, MNRAS, 521, 2103
- Manchester R. N. et al., 2013, Publ. Astron. Soc. Aust., 30, e017 Marshall F. E., Gotthelf E. V., Zhang W., Middleditch J., Wang Q. D., 1998,
- ApJ, 499, L179 Moore C. J., Cole R. H., Berry C. P. L., 2014, Class. Quantum Gravity, 32, 015014
- Morsink S. M., Rezania V., 2002, ApJ, 574, 908
- Nissanke S., Holz D. E., Hughes S. A., Dalal N., Sievers J. L., 2010, ApJ,
- Oertel M., Hempel M., Klaehn T., Typel S., 2017, Rev. Mod. Phys., 89, 015007
- Owen B. J., 2010, Phys. Rev. D, 82, 104002
- Owen B. J., Lindblom L., Cutler C., Schutz B. F., Vecchio A., Andersson N., 1998, Phys. Rev. D, 58, 084020
- Özel F., Freire P., 2016, A&A, 54, 401
- Pang P. T. H., Tews I., Coughlin M. W., Bulla M., Broeck C. V. D., Dietrich T., 2021, ApJ, 922, 14
- Papaloizou J., Pringle J. E., 1978, MNRAS, 182, 423
- Passamonti A., Haskell B., Andersson N., Jones D. I., Hawke I., 2009, MNRAS, 394, 730
- Pietrzyński G. et al., 2019, Nat., 567, 200
- Prix R., 2007, Phys. Rev. D, 75, 023004
- Punturo M. et al., 2010, Class. Quantum Gravity, 27, 084007
- Rajbhandari B., Owen B. J., Caride S., Inta R., 2021, Phys. Rev. D, 104, 122008
- Rezzolla L., Lamb F. K., Shapiro S. L., 2000, ApJL, 531, L139
- Rezzolla L., Lamb F. K., Marković D., Shapiro S. L., 2001a, Phys. Rev. D, 64, 104013
- Rezzolla L., Lamb F. K., Marković D., Shapiro S. L., 2001b, Phys. Rev. D, 64, 104014
- Riles K., 2023, Living Rev. Relativ., 26, 3
- Saleem M. et al., 2021, Class. Quantum Gravity, 39, 025004
- Schutz B. F., 1986, Nature, 323, 310
- Schutz B. F., 2011, Class. Quantum Gravity, 28, 125023
 - Sieniawska M., Jones D. I., 2021, MNRAS, 509, 5179
- Sieniawska M., Jones D. I., Miller A. L., 2023, MNRAS, 521, 1924
- Traversi S., Char P., Pagliara G., 2020, ApJ, 897, 165
- Usman S. A., Mills J. C., Fairhurst S., 2019, ApJ, 877, 82
- Vallisneri M., 2008, Phys. Rev. D, 77, 042001
- Yagi K., Yunes N., 2013a, Phys. Rev. D, 88, 023009
- Yagi K., Yunes N., 2013b, Sci., 341, 365
- Yagi K., Yunes N., 2017, Phys. Rep., 681, 1
- Yoshida S., Lee U., 2000, Astrophys. J., Suppl. Ser., 129, 353

This paper has been typeset from a TEX/LATEX file prepared by the author.